



# Numerical study of transient instabilities in reverse-roller coating flows

Numerical study  
of transient  
instabilities

375

M.S. Chandio and M.F. Webster

*Institute of non-Newtonian Fluid Mechanics,  
Department of Computer Science, University of Wales Swansea,  
Swansea, UK*

**Keywords** Numerical simulation, Finite elements, Free form surfaces

**Abstract** A semi-implicit Taylor-Galerkin/pressure-correction algorithm of a transient finite element form is applied to analyse the flow instabilities that commonly arise during reverse-roller coating. A mathematical model is derived to describe the solvent coating applied to the underside of the sheet, assuming that the lacquer is a Newtonian fluid and considering the flow between application roller and foil. Here, we have investigated the effects of temporal instabilities, caused by adjustment of nip-gap width and foil-position, extending our previous steady-state analysis. Foil shifting is found to have a significant influence upon pressure and lift on the foil, drag on the roller, and free coating profiles. This would result in process instabilities, such as chatter and flow-lines. In contrast, nip-gap adjustment has no influence on the coating finish.

## 1. Introduction

This work addresses the reverse-roller coating between an application roller and a sheet-foil. The study of roller-coating with free-surfaces is an important topic that commonly arises in many industrial areas, particularly those associated with the production of tape, film and printing situations. Over the past two decades, roller-coating processes have been analysed extensively, involving experimental, analytical and computational studies. Forward roller-coating has attracted the attention of many research groups. Forward roller-coating and reverse roller-coating processes are distinguished by counter-rotating and co-rotating moving rolls, respectively. The ultimate aim of such procedures is to deposit a thin uniform layer to a continuous flexible substrate. There is little reported in the literature concerning reverse roller-coating between foil and roller, taking into account start-up behaviour and time-dependent instabilities. Hence, we briefly comment upon related studies.

Cohu and Magnin (1997) conducted experimental investigations into forward roller-coating of Newtonian fluids between deformable rolls. These authors observed that the decrease of the thickness of a rubber cover on a roller, below a critical value, tends to decrease the coating thickness significantly. Based on forward roller-coating Carvalho and Scriven (1997a) have argued in



The authors wish to express their thanks to Alcoa Manufacturing Ltd. for their financial support and practical guidance throughout this study.

their numerical work, that the upstream free-surface touches the top roll, and air is trapped between the roll surface and the coating liquid. Consequently, the coated film that is delivered is defective. Various flow states are described, both metered and pre-metered, by moving the rolls apart and bringing them together. As the rolls are pushed together, the gyre moves upstream towards the inlet plane. These authors have replaced the fixed inlet film thickness condition with a weighted kinematic residual, which guarantees that the flow is normal to the inlet boundary in some averaged sense.

Carvalho and Scriven (1997b) conducted a similar study, where the stability of the given system to transverse perturbation is analysed theoretically, numerically and experimentally. A mathematical model is presented to predict the critical *capillary* number for the onset of ribbing, concluding that roll cover deformation alters the wavelength of the ribbing pattern. Roll cover softness is related to increasing the solids elasticity number. Increasing the elasticity number of the soft roll cover, largens the wavelengths and diminishes wave numbers, and this stimulates a faster increase in instability modes. The consequence is a larger ribbing wavelength and the retardation of the levelling rate. To obtain a desired coating thickness, an appropriate criterion must be selected to pinpoint the choice of roll covers.

Fourcade *et al.* (1999) investigated a coating operation of a reverse roller-coating process between two rollers. The main attention is focused on the deformation of the elastomer on the coated roll. The pressure is reported to increase in the converging section of the gap, and reaches its peak slightly to the left of the contact point of the rollers. The largest deformation of the elastomer cover of  $70\ \mu\text{m}$  is observed to occur at the location where the pressure reaches a maximum. The lower the gap size, the higher the pressure peak that is observed. Chen and Scriven (1988) chose to set the inflow rate based upon the incoming liquid layer, treated as a plug flow following Benjamin (1994). According to Benjamin, in meniscus coatings, the flow is always pre-metered and, therefore, imposing a velocity profile at the inflow boundary is a satisfactory boundary condition.

One difficulty with computer modelling of such coating scenarios lies in the treatment of moving free-surface problems, accommodating kinematic and dynamic boundary conditions on the free-surface and the simultaneous calculation of its position. For the last two decades the finite element method has played an important role in simulating the flow of fluids subject to free surfaces. Literature of relevance on this topic can be found in (Keunings, 1986; Sizaire and Legat, 1997; Tanner *et al.*, 1975; Silliman and Scriven, 1980; Saito and Scriven, 1981; Ramaswamy, 1990; Hirt *et al.*, 1974; Sato and Richardson, 1994; Chandio and Webster, 2001; Regalt *et al.*, 1993). For details on this issue we refer to our previous steady analysis (Chandio and Webster, 2001), where attention is focused upon the flow patterns that result and variation in pressure, lift and drag at various roll and foil-speeds. Here, a finite element

simulation of the roller-coating process is presented, based on a semi-implicit Taylor-Galerkin/Pressure-correction algorithm (Townsend and Webster, 1987; Hawken *et al.*, 1990; Carew *et al.*, 1993). For free-surface prediction, we use kinematic boundary adjustment with a mesh-stretching algorithm.

The main purpose of the present work is to provide a description of reverse roller-coating flows, accounting for the parameters affecting the coating process, and, in particular, those of most practical significance. Major attention is focused upon flow instabilities, seeking to investigate transient effects and the influence these have upon typical processing instabilities. Various nip-flow conditions are considered, to take into account some leakage at the nip and to provide consistent local settings. The effects of such leakage upon the flow are determined. In particular, temporal variations between leakage and no-leakage states are simulated. Finally, temporal foil-shifting is investigated. Foil-shifting is invoked in two distinct forms: first, via global uniform shifting, and second, through more local adjustment. Results are interpreted through pressure, lift and drag, quantified locally, and through the influence of such temporal fluctuations upon the free-surface shape of the lacquer coating.

## 2. Problem specification and governing equations

The isothermal and two-dimensional coating flow of Newtonian liquid is considered. The system consists of a roller of radius  $r_1$ , rotating at speed  $U_{\text{roll}}$ , applying a coating to the underside of the alloy sheet of thickness  $G(x, t)$ . The sheet rests on both the roller and the thin film of fluid trapped between the roller and the sheet. The sheet moves with speed  $U_{\text{foil}}$  in the horizontal direction (negative  $x$ ) and the problem is posed in a Cartesian frame of reference. A schematic diagram of the flow is illustrated in Figure 1.

The isothermal flow of Newtonian fluid is governed by equations for the conservation of mass and transport of momentum. In the absence of body forces, the system may be expressed in the form

$$\rho \frac{\partial u}{\partial t} = \nabla \cdot \tau - \rho u \cdot \nabla u - \nabla p \quad (1)$$

$$\nabla \cdot u = 0 \quad (2)$$

where  $\rho$  is the fluid density,  $t$  is the time,  $u(x, t)$  is the fluid velocity and  $p$  is the isotropic pressure. For Newtonian flows, the stress  $\tau$  is defined via a constant viscosity  $\mu$ , and the rate of deformation tensor  $\mathbf{D}$ ,

$$\tau = 2\mu\mathbf{D} \quad (3)$$

$$\mathbf{D} = \frac{L + L^t}{2} \quad \text{and} \quad L = \nabla u. \quad (4)$$

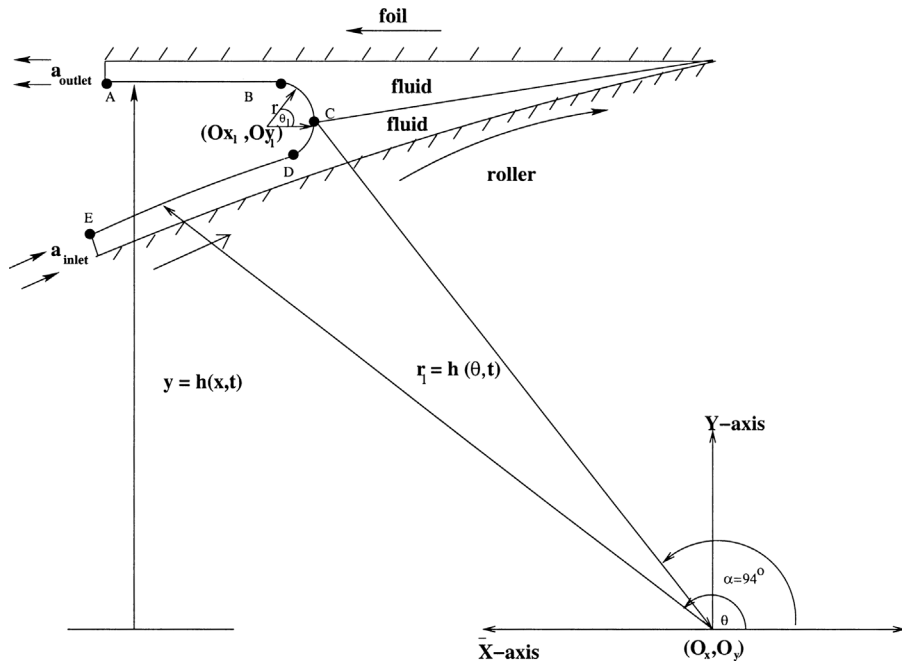


**Figure 1.**  
Schematic flow diagram

For a Newtonian fluid, the Navier-Stokes equations can be recovered, by recourse to the continuity equation (2),

$$\rho \frac{\partial u}{\partial t} = \mu \nabla^2 u - \rho u \cdot \nabla u - \nabla p \tag{5}$$

where  $\mu \nabla^2 u$  is a diffusion term.

For conciseness and convenience, adopting characteristic scales on velocity,  $U$  (standard foil speed), length,  $L$  (steady-state coating thickness, no leakage) and viscosity,  $\mu$ , we may define non-dimensional variables  $u = Uu^*$  and  $p = [\mu U/L]p^*$ . Hence, we may define an equivalent non-dimensional system of equations to (2) and (5), discarding the  $*$  notation for clarity of representation,

$$\text{Re} \frac{\partial u}{\partial t} = \nabla^2 u - \text{Re} u \cdot \nabla u - \nabla p, \tag{6}$$

$$\nabla \cdot u = 0,$$

where the non-dimensional group Reynolds number is defined as  $\text{Re} = \rho UL/\mu$ .

For the solution of the given system of governing equations, both initial and boundary conditions are required. Initial conditions can be formed by prescribing initial values for the primitive field variables at  $t = 0$ ,

$$U(x, t) = u_0(x, 0),$$

$$p(x, t) = p(x, 0).$$

Conditions at the free-surface require a normal constraint,

$$p + \tau_{nn} = -p_0 + \sigma_s \beta, \quad (7)$$

whilst the absence of friction ensures the tangential constraint,

$$\tau_{nt} = 0. \quad (8)$$

Here,  $\tau_{nn}$ ,  $\tau_{nt}$  are normal and tangential stress components, respectively,  $p_0$  is atmospheric pressure and  $p$  local pressure,  $\sigma_s$  is a surface tension coefficient and  $\beta$  is the mean curvature of the free-surface (Saito and Scriven, 1981). Remaining boundary conditions are taken of no-slip on roller and foil, uniform flow at inlet on the roller and outlet on the foil. In a no-leakage state, there is vanishing flux across the nip. No-slip boundary conditions for the flow on solid surfaces are taken as:

$$\begin{aligned} \text{on foil : } U_x &= -\bar{U}_{\text{foil}}, \quad U_y = 0; \\ \text{on roller : } U_x &= U_{\text{roll}} \cos\theta, \quad U_y = U_{\text{roll}} \sin\theta, \end{aligned} \quad (9)$$

where  $U_{\text{roll}} = R\omega$ ,  $R$  is the radius and  $\omega$  the angular rotation rate of the roller.

The evolving position of the free-surface, is unknown apriori and must therefore be computed as part of the solution. In this respect, we appeal to the kinematic boundary conditions (Keunings, 1986). On flat free-surface boundaries (lines at constant  $y$ ) this leads to:

On flat free-surface boundaries (lines at constant  $y$ ):

$$\frac{\partial h}{\partial t} = -U_x \frac{\partial h}{\partial x} + U_y, \quad (12)$$

On the curved meniscus boundary section (lines at fixed azimuthal angle  $\theta$  setting):

$$\frac{\partial h}{\partial t} = -U_\vartheta \frac{1}{r} \frac{\partial h}{\partial \vartheta} + U_r \quad (11)$$

A combination of both equations (10) and (11) is required for the current flow problems.

### 3. Finite element analysis

A Taylor-Galerkin algorithm is used to solve the governing equations (6). This involves a two-step Lax-Wendroff approach, based on a Taylor series expansion up to second order in time, to compute solutions through a time

stepping procedure. A two-step pressure-correction method is applied to handle the incompressibility constraint. Employing a Crank-Nicolson treatment on diffusion terms, produces an equation system of three fractional-staged equations (Hawken *et al.*, 1990). In stage one a non-solenoidal velocity field  $u^{n+1/2}$  and  $u^*$  are computed via a predictor-corrector doublet. The resulting mass-matrix bound equation is solved via a Jacobi iteration. With the use of  $u^*$ , the second stage computes the pressure difference,  $p^{n+1} - p^n$ , via a Poisson equation, and the application of a direct Choleski solver. The third stage completes the time step loop, calculating the end-of-time-step solenoidal velocity field  $u^{n+1}$ , again by a Jacobi iterative solver. Full details upon this implementation may be found in Townsend and Webster (1987) and Hawken *et al.* (1990).

Following the notation of Cuvelier *et al.* (1986), the velocity and pressure fields are approximated by  $U(x, t) = U^j(t) \phi_j(x)$  and  $P(x, t) = P^k(t) \psi_k(x)$ , where  $U$  and  $P$  represents the vectors of nodal values of velocity and pressure, respectively, and  $\phi_j$  are piecewise quadratic and  $\psi_k$  linear basis functions on triangles.

The fully-discrete semi-implicit Taylor-Galerkin/pressure-correction system of equations may be expressed in matrix form:

$$\text{Stage 1a. } \left( \frac{2\text{Re}}{\Delta t} M + \frac{1}{2} S \right) (U^{n+1/2} - U^n) = \{ - [S + \text{Re } N(U)]U + L^T P \}^n$$

$$\text{Stage 1b. } \left( \frac{\text{Re}}{\Delta t} M + \frac{1}{2} S \right) (U^* - U^n) = (-[SU + L^T P]^n - [\text{Re } N(U)U]^{n+1/2}) \quad (12)$$

$$\text{Stage 2 } K(P^{n+1} - P^n) = -\frac{2}{\Delta t} \text{Re } LU^*$$

$$\text{Stage 3 } \frac{\text{Re}}{\Delta t} M(U^{n+1} - U^*) = \frac{1}{2} L^T (P^{n+1} - P^n),$$

where  $M$ ,  $S$ ,  $N(U)$ ,  $L$ , and  $K$  are consistent mass matrix, momentum diffusion matrix, convection matrix, pressure gradient matrix and pressure stiffness matrix, respectively. With elemental fluid area  $d\Omega$ , such matrix notation implies,

$$M_{ij} = \int_{\Omega} \phi_i \phi_j d\Omega,$$

$$N(U)_{ij} = \int_{\Omega} \phi_i \left( \phi_1 U_1 \frac{\partial \phi_j}{\partial x} + \phi_1 U_1 \frac{\partial \phi_j}{\partial y} \right) d\Omega,$$

$$((L_k)_{ij}) = \int_{\Omega} \frac{\partial \phi_j}{\partial x_k} d\Omega,$$

$$K_{ij} = \int_{\Omega} \nabla \psi_i \nabla \psi_j d\Omega,$$

$$S_{ij} = \int_{\Omega} \nabla \phi_i \nabla \phi_j d\Omega.$$

For the computation of the free-surface, we have used the kinematic boundary conditions (Keunings, 1986; Sizaire and Legat, 1997). These can be expressed in a general discrete variational form:

$$\begin{aligned} \text{Stage 4} \quad & \frac{1}{\Delta t} \int_{\Gamma} (\psi_i + (\alpha_1 + u \cdot \nabla \psi_i)) (\psi_k + (\alpha_2 + u \cdot \nabla \psi_k)) \Delta H_k^{n+1} d\Gamma_F \\ & - \int_{\Gamma} (\psi_i + (\alpha_1 + u \cdot \nabla \psi_i)) u \cdot \nabla \psi_k H_k^n d\Gamma_F \end{aligned} \quad (13)$$

adopting notation for time-step,  $\Delta t$ , interpolant,  $H^n(x)$ , interpolating functions,  $\psi_k(x)$ , and nodal solution increment,  $\Delta H_k^n$ ,

$$H^n(x) = H_k^n \psi_k(x) \text{ and } \Delta H_k^{n+1} = (H_k^{n+1} - H_k^n). \quad (14)$$

The scheme expressed in (13) is quite flexible, where we define generalized scalar factors  $\alpha_i$  to switch between Galerkin and Streamline-Upwind Petrov-Galerkin (SUPG) (explicit and implicit) schemes, as and when required. A free-surface boundary segment is indicated by  $\Gamma_F$ , over which quadrature may be established. In equation (13), the generalized form of convective term is represented, subsuming either equation (10) or (11), depending upon the particular boundary segment under consideration. We have found it most effective to use  $\alpha_1 = \alpha^n$  (an SUPG parameter<sup>3</sup>) and  $\alpha_2 = \Delta t/2$  to recover an implicit SUPG scheme. Then, both  $\psi_i$  (and  $\psi_k$ ) are taken as linear functions on straight-sided boundary element sections.

#### 4. Numerical results and discussion

A standard foil-speed setting of one unit and roller speed, 90 per cent of foil-speed, constitutes the base scenario around which solutions are sought. Results are reported in non-dimensional form for convenience of representation. The mesh used is displayed in Figure 2, with 2925 nodes, 1302 elements and 6662 degrees of freedom. A typical steady-state flow pattern is shown in Figure 2d, represented in space-filled motion blur format, based on the velocity vector field (Chandio and Webster, 2001) (colour implies speed magnitude; red-fast, green-medium, blue-slow). In this section, we are particularly interested in

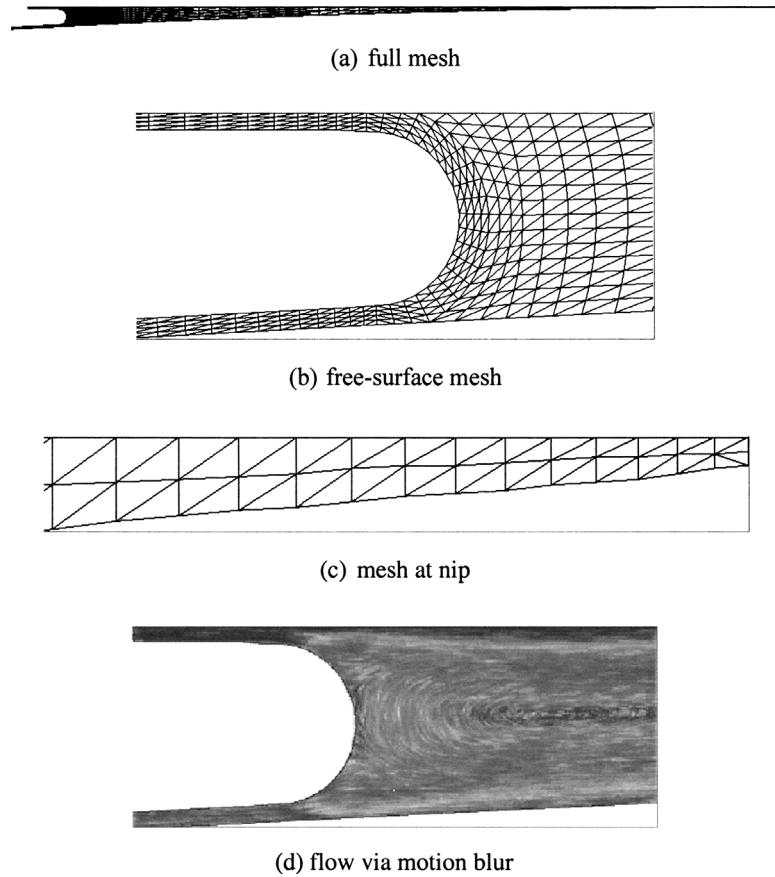


**Figure 2.**  
Finite element mesh  
sections and flow  
representation

pressure maxima across the nip region (see Figure 2c), lift is considered along the foil surface and drag on the roller. For a Newtonian fluid, the lift ( $L_{\text{foil}}$ ) and drag ( $D_{\text{roller}}$ ) are given through the following expressions:

$$L_{\text{foil}} = \int_{\Gamma_{\text{foil}}} \{ -p \sin\theta + \tau_{xy} \cos\theta + \tau_{yy} \sin\theta \} d\theta = \int_{\Gamma_{\text{foil}}} L_f d\theta \quad (14)$$

$$D_{\text{roller}} = \int_{\Gamma_{\text{roller}}} \{ -p \cos\theta + \tau_{xx} \cos\theta + \tau_{xy} \sin\theta \} d\theta = \int_{\Gamma_{\text{roller}}} (-D_R) d\theta \quad (15)$$

where  $\tau = 2\mu D$ , so that  $L_f$  and  $D_R$  are distributional quantities on the respective surfaces (unassigned where possible)

Results are categorised into different sections. The first deals with the variation in nip velocity and pressure profile conditions. This is in order to choose a suitable velocity profile at the nip, prior to investigating temporal

changes. A second section is devoted to the study of temporal changes in leakage, but without foil-shifting. This allows us to interpret transient variations of pressure at the nip. Global foil-shifting at steady-state is studied in a third section. Lastly, we consider foil-shifting locally and globally in time. All settings discussed are concerned with nodal positions  $N_2$ ,  $N_4$  and  $N_5$ . No-slip boundary conditions (9) apply on nodes  $N_1$  and  $N_3$ , see Figure 3. In the standard no-leakage setting, fluid is not permitted to traverse through the nip-gap. So fluid travels along the roller and is carried away by the foil. The parameter of importance here in the numerical algorithm, is the time-step ( $\Delta t$ ). This is chosen for pragmatic reasons, to satisfy accuracy and stability constraints, as 0.005 units.

#### 4.1 Variation in nip flow conditions

Prior to analysing flow instabilities, it is instructive to choose an appropriate velocity profile to allow a degree of leakage at the nip. This automatically implies flow, out through the nip, that must be counterbalanced by inflow/coatoutlet-flow. Temporal adjustments to nip boundary conditions are consigned to later sections. There is no flow (leakage) through the nip under standard settings. No-slip boundary conditions apply on the foil and roller nodes at the nip, see Figure 3a. A typical schematic diagram of plug and Couette flow is shown in Figure 4 (vanishing vertical velocity). Natural unconstrained boundary conditions are referred to as free, and strong constrained boundary conditions as fixed. In Figure 5, various examples of horizontal velocity component profiles of plug and Couette-type are displayed over a fixed nip-gap width. At nodal positions  $N_2$ ,  $N_4$ ,  $N_5$  corresponding values are charted in Tables I and II. For stable numerical calculations, one has to treat the severe conditions at the nip with care. It is found necessary to constrain some solution variables. Imposing either opposing plug (setting I) or Couette flow profiles (setting II and III), provides results (pressure, lift and drag) that lie close to the standard no-leakage setting. Couette flow setting III, is held to be more physically representative, see Figure 5c and Tables I and II.

Figure 6 shows the distributional pressure ( $P_f$ ), lift ( $L_f$ ) along the foil and drag ( $D_R$ ) along the roller. The section of the foil considered would amount to a distance of 500 units from the nip. The maximum lift around  $82 \times 10^3$  units, is observed on the nip outlet with the Couette flow setting (see Figure 5c). With the standard no-leakage setting, a negligible leakage is observed through the nip-gap, inherent to the FE discretisation, and the lift value is  $63 \times 10^3$  units. With a Couette flow setting, a larger degree of leakage is allowed that generates larger lift than the standard setting. Differences in total lift across the various settings are practically identical, as shown in Table II. As pressure decreases, lift and drag also decrease, see Table II. The drag on the roller is fairly small along most of the roller-length, see Figure 6. The distributional drag on the roller,  $D_R$ , is negated to imply physical meaning through magnitude, as with

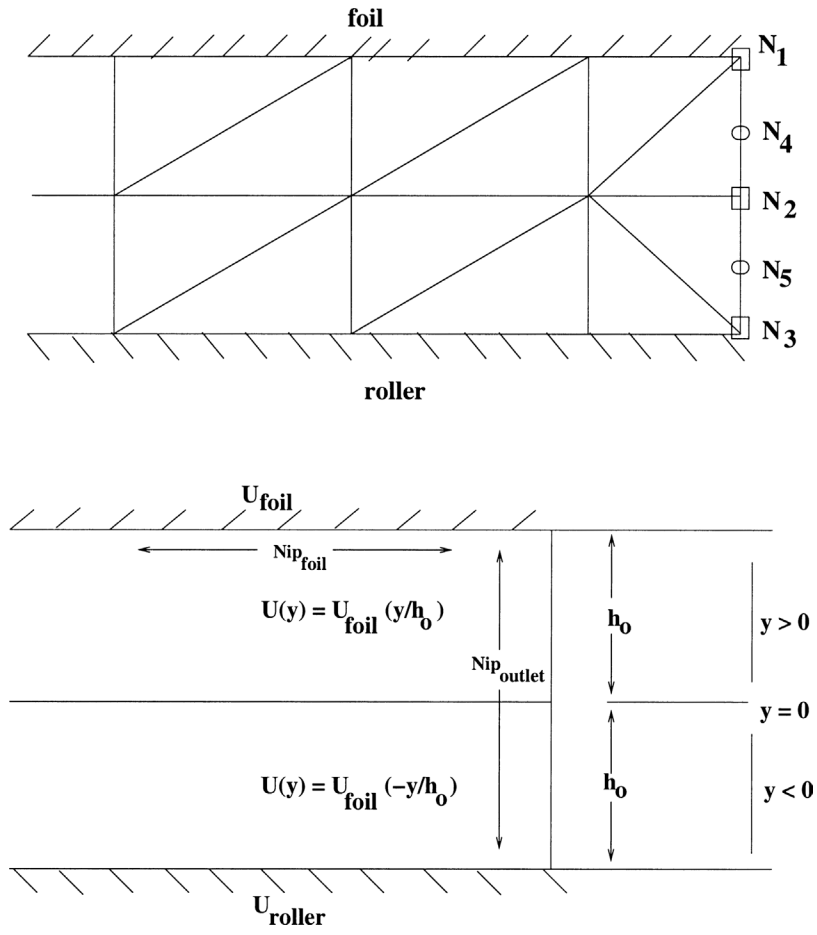


**Figure 3.**  
Nip mesh and velocity  
conditions

pressure.  $D_R$  first rises along the roller travelling towards the nip, then declines around 100 units from the nip, dropping into negative values close to the nip. The sudden kinematic changes at 10 units from the nip cause a rapid rise in  $D_R$ , where large shear-rates are observed (Chandio and Webster, 2001). Such negative drag values can be attributed to the increase in cross-stream flux close to the nip (that has generated negative shear-stress) before it merges with the imposed Couette-flow profile. These sharp adjustments into negative drag values vanish as nip-gap width increases, see Figures 9–11. Since these changes are purely local and are restricted to the nip region, so the free-surface remains unaffected. Maxima of forces in Table II, are shown over  $Nip_{\text{outlet}}$  and  $Nip_{\text{foil}}$  regions, defined in Figure 3b.

4.2 Temporal adjustment of nip conditions

The main purpose here is to evaluate the effect of temporal leakage adjustment upon the pressure and lift acting on the foil, with a fixed nip-gap width. This is performed through variations in conditions across the time steps with a corresponding sensitivity analysis. The pressure variation is observed at various time step setting protocols, by switching between standard setting (no leakage) and Couette flow setting (leakage setting III, see Table I) in time. This applies to all leakage settings adopted below. Pressure, lift and drag reflect almost identical results, to those at standard settings, see Figure 7 and Table III. With temporal adjustment of nip conditions, but without foil movement, we observe in Figure 8, a trend towards a constant periodicity (regular frequency) in the temporal change of the pressure at the nip. There is only minimal pressure variation and this is local to the nip. Hence, there is hardly any influence over the coating free-surface profile on the foil.

4.3 Global foil-shifting

Thus far, we have observed that there is only minimal pressure variation and this is local to the nip. Hence, foil/meniscus pressure profiles remain unaffected. Next, the effects of foil-shifting are investigated in response to flow-instabilities. Nip-gap size is increased by shifting the foil vertically upwards,

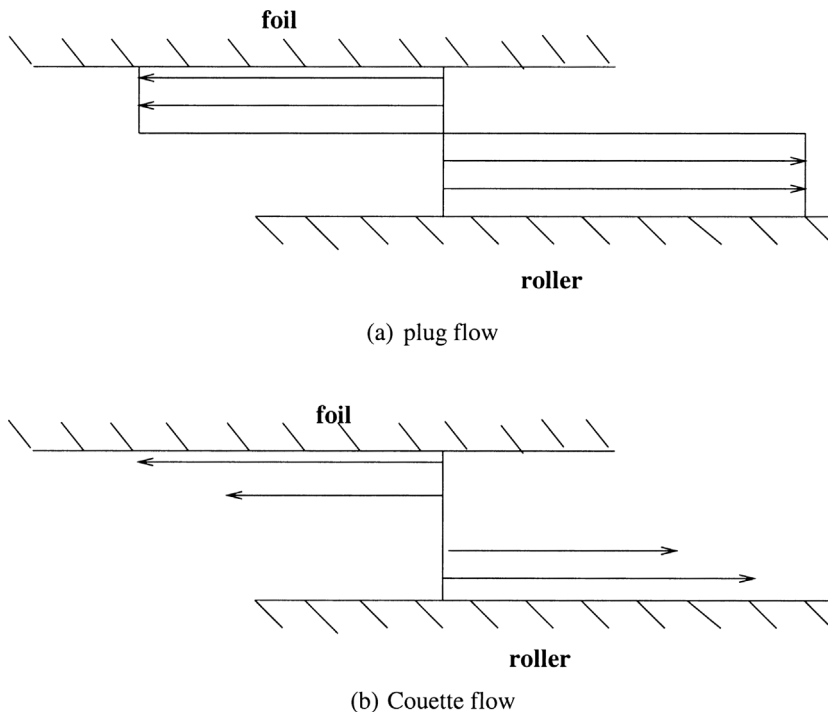


**Figure 4.**  
Schematic diagram of  
(a) plug and (b) Couette  
flow velocity profiles  
at nip



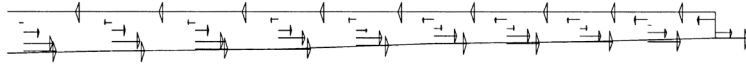
(a)  $U_{N4} = U_{N1}$ ;  $U_{N5} = U_{N3}$ ;  $U_{N2} = 0$ ;  $P_{N2}$  free; setting I



(b)  $U_{N4} = U_{foil} \frac{1}{h_0}(y)$ ;  $U_{N5} = U_{roller} \frac{1}{h_0}(-y)$ ;  $U_{N2}$  free; setting II

**Figure 5.**

Flow pattern with various nip velocity/pressure settings



(c)  $U_{N4} = U_{foil} \frac{1}{h_0}(y)$ ;  $U_{N5} = U_{roller} \frac{1}{h_0}(-y)$ ;  $U_{N2} = 0$  fixed; setting III

**Table I.**

Nip conditions; velocity

Settings	U		
	N <sub>2</sub>	N <sub>4</sub>	N <sub>5</sub>
Standard	0	0	0
I (constrained u)	0	$U_{N1}$	$U_{N3}$
II (constrained u at N <sub>4</sub> , N <sub>5</sub> )	-1.8	$U_{foil}(h_0 - y)$	$U_{roller}(h_0 + y)$
III (constrained u)	0	$U_{foil}(h_0 - y)$	$U_{roller}(h_0 + y)$

**Table II.**

Nip conditions; maxima in P, lift (on foil) and drag (on roller), values  $\times 10^3$  units

Settings	$P_{max}$				
	Nip <sub>outlet</sub>	Nip <sub>foil</sub>	Lift	Drag	
standard	160	160	1311	1.30	
I	152	150-121	1286	1.30	
II	85	95-102	1286	1.30	
III	156	153-123	1298	1.30	

uniformly across its length, relocating at a specified new nip-width, taken as a function of time-step variation.

4.3.1 *Shift and solve to steady state.* The variation of leakage is considered at various nip-width settings. At 2 per cent nip-width, the pressure peak at the nip has decreased by 83 per cent to that of the standard setting result. Correspondingly, there is a decline of similar form in lift. However, these settings have no significant influence on the drag, see Table IV. It is to be noted

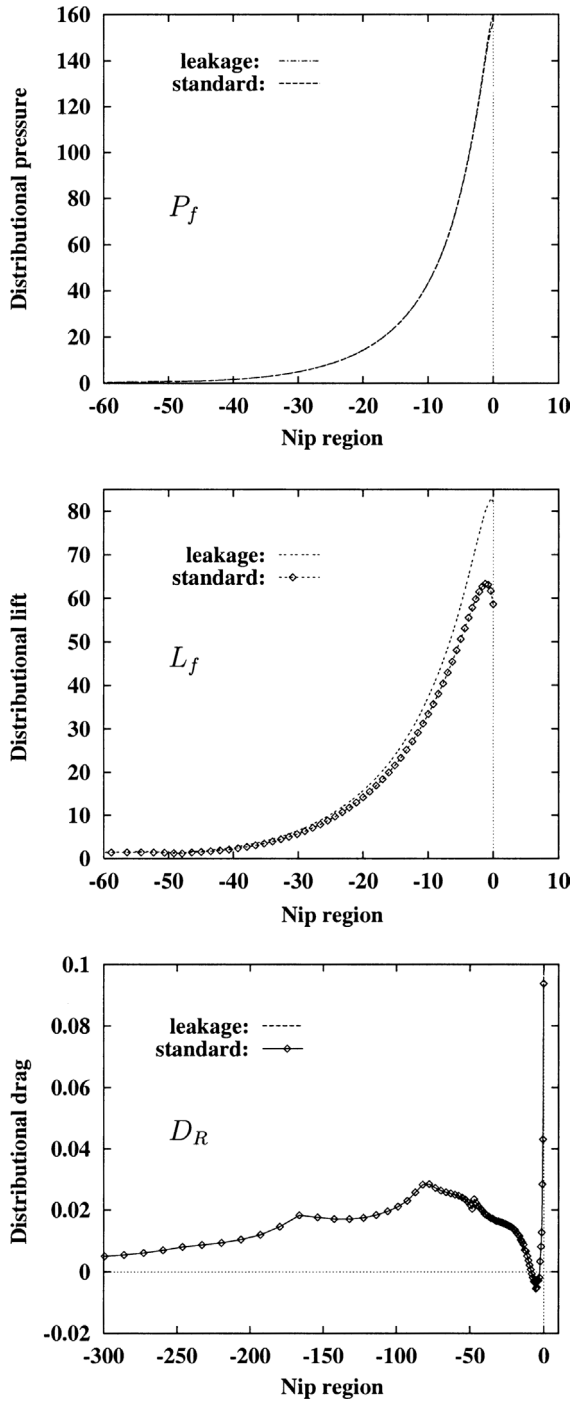


**Figure 6.**  
Distributional pressure  
( $P_f$ ) and lift ( $L_f$ ) along foil,  
and drag ( $D_R$ ) on roller,  
(values  $\times 10^3$ ).

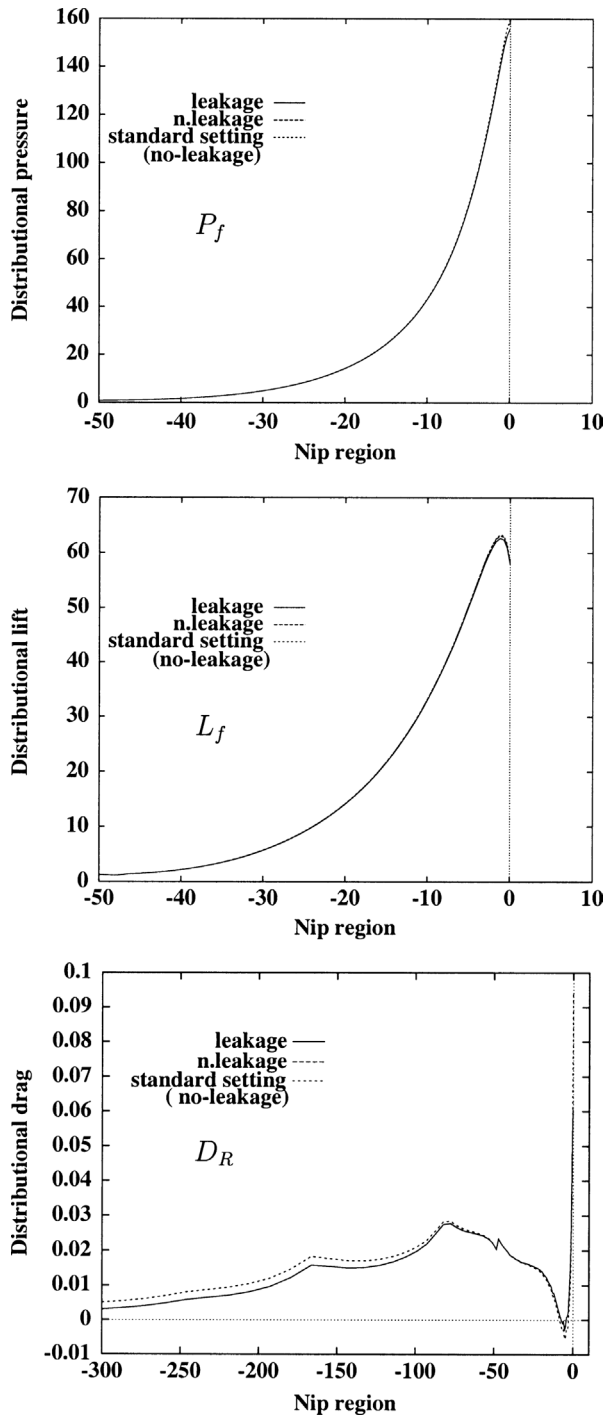


**Figure 7.**  
Temporal leakage  
adjustment: settled  
distributional pressure  
( $P_f$ ) and lift ( $L_f$ )  
along foil,  
and drag ( $D_R$ ) on roller,  
values  $\times 10^3$ ,  $10_1 - 10_{nb}$ ,  
true for all protocols

that drag is a trivial quantity in the present study. Locally to the nip, lift decreases by 68 per cent and drag by 60 per cent. This is shown to be largely restricted to the nip region, see Figure 9. Similarly, at 3 per cent nip-width, pressure maxima at the nip have decreased by 90 per cent and lift by 78 per cent, see Table IV.

Such global foil shifting, considered to steady state in time, hardly affects the outlet/meniscus flow. This is entirely reasonable as the adjustment incurs such minor leakage, which hardly reduces the flow rate at the outlet, i.e. coating on the foil. We may discern the influence of nip-width adjustment, prior to transient fluctuations. That is, in contrast to the Couette flow studies of section 4.2, where an increasing degree of leakage also applied, but imposed for a 1 per cent fixed nip-gap width. The findings are broadly similar with localized force balance adjustments restricted to the nip, so that the free-surface remains unaffected. Hence, an important point to note is that changes imposed in nip-gap width have influence around the nip region only.

*4.3.2 Temporal adjustment of foil position.* Here, foil vibration is performed at set time-steps intervals. So, for example, the foil is allowed to move up/down by creating/removing a gap between roller and foil, after every  $N$  alternate time-steps. Effectively the foil is either rising off/laying on the roller. Nip conditions that switch between different foil positions are taken as of subsection 4.2. The results presented below are associated with data sampled when the foil is in a shift-up mode, and are compared with the standard setting. The foil is shifted at different time-step protocols. The drop of pressure is related not only to nip-width, but also to foil shift-up time. Increment in foil shift-up time retards the pressure and lift considerably, see Table V. It is found helpful to consider integrated quantities on surfaces in their contributions per unit area (distributional), to appreciate their spread. As regards distributional

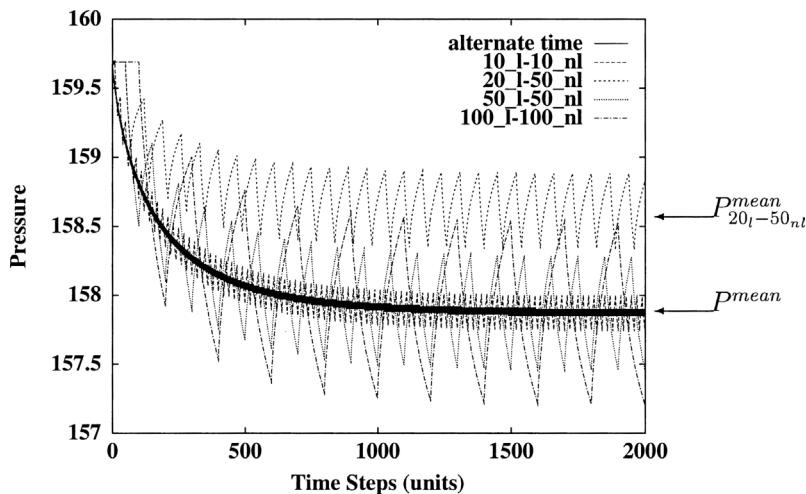


**Figure 8.**  
Temporal leakage  
adjustment, pressure  
at nip node  $N_1$ ,  
values  $\times 10^3$

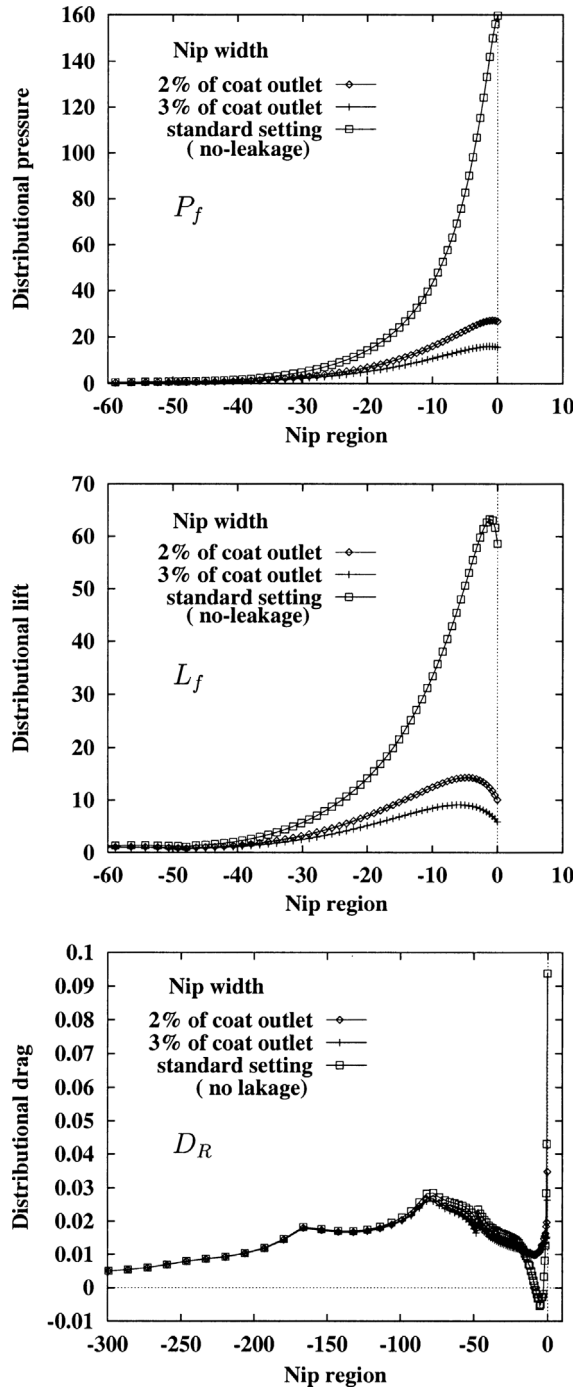


**Figure 9.**  
Global foil shifting,  
steady state:  
distributonal pressure  
( $P_f$ ) and lift ( $L_f$ ) along foil,  
and drag ( $D_R$ ) on roller,  
values  $\times 10^3$ .

pressure/lift on the foil and drag on the roller in a no-leakage (nl) state, it is noted that, the greater time-step variation protocol ( $100_l - 100_{nl}$ ) does attain a level, close (within 10 per cent) to that of the standard nl-setting, see Figures 10 and 11. Pressure profiles, are illustrated in contrast to the standard setting. The decline and rise of pressure is clearly exhibited, at leakage (Couette velocity profile) and no-leakage (standard setting) states, across time-step variations, see Figure 11. On average, pressure and lift decrease, with increasing nip-width, see Table V.

Temporal variation in pressure is sampled at a single point, on the foil, at the nip region, see Figure 12. Pressure is observed to be a direct sensor of lift, and hence, the choice to plot this quantity. The rise and fall of pressure is clearly apparent at alternate specified time-steps. Therein, we see regular periodicity in pressure sampled at the nip. The sharpness of the profiles, over an individual period is associated with high frequency protocols. At low frequency, this sharpness is dispersed, such as with the  $100_l - 100_{nl}$  protocol. This is so, even with increase in nip-gap width cases.

We comment that by employing an appropriate nip-width setting, one can control the threshold level of pressure. This may be used as a mechanism to constrain lift, which mitigates foil-vibration. The plots of Figure 13 for  $P_{\min}(t)$  in a leakage-state, for 2 per cent, 3 per cent and 5 per cent settings, at high and low frequency protocols, indicate corresponding settling times (to a steady-position). These are more rapid at larger nip-widths. Permitting a leakage/no-leakage pattern over a specified time-step variation sequence generates foil vibration, which creates oscillations at the flow-outlet free-surface region on the foil. When the roller rotates at a certain speed, the fluid exerts a potentially increasing force upwards on the foil, and the lift/pressure forces reach a maximum level. This level is sufficient to push the foil upwards, creating a larger gap between the roller and the foil at the nip region. Accordingly, a small degree of leakage may occur. The pressure/lift forces exerted by the fluid subsequently diminish in time and have the effect of resettling the foil back onto the roller. This is a transient (periodic) phenomenon. During the process of foil shifting (up/down), one may equate and balance the respective flow rates between in-flow, coat-outlet flow and nip-outlet flow. The film-layer thickness varies, in a uniform manner, along its length. When there is no-leakage, the required wet film thickness implies a flow rate balance between in-flow and coat-outlet flow. When the foil rises off the roller, a minimal degree of leakage, between 1 per cent–3 per cent of the coat-outlet, is allowed through the nip-gap. This affects the wet film-thickness, reducing its thickness by the same order as that of the leakage, so that, now the coat-outlet flow rate is decreased by the leakage flow rate at the nip.

In Figures 14 and 15, free-surface profiles are given at 2 per cent nip-width for the  $100_l - 100_{nl}$  protocol. Identical free-surface profiles are obtained for other protocols. Wave patterns on the free-surface are apparent. The intensity of such

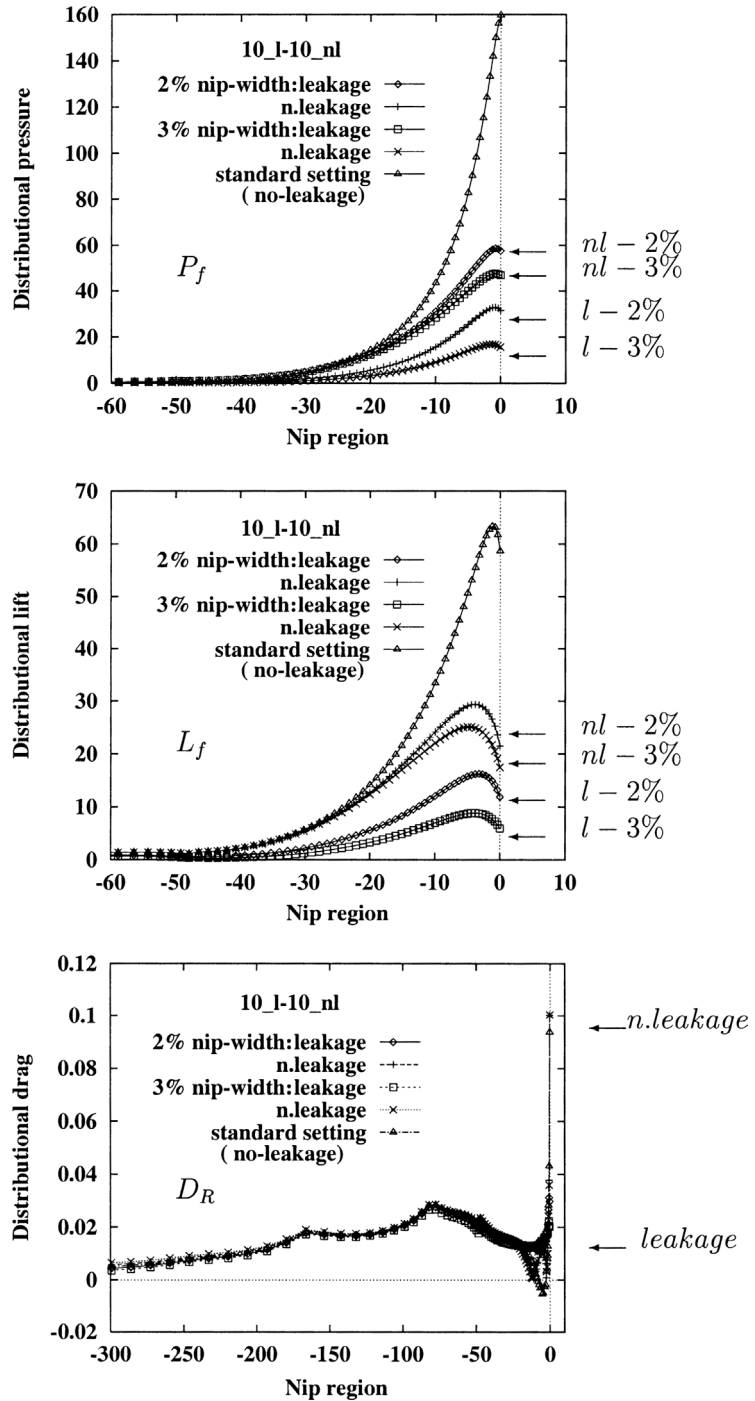


**Figure 10.** Global foil shifting, temporal variations, settled distributional pressure ( $P_f$ ) and lift ( $L_f$ ) along foil, and drag ( $D_R$ ) on roller, values  $\times 10^3$  at  $L$  per cent nip-width of  $coat_{outlet}$ ,  $10_l - 10_{nl}$  protocol

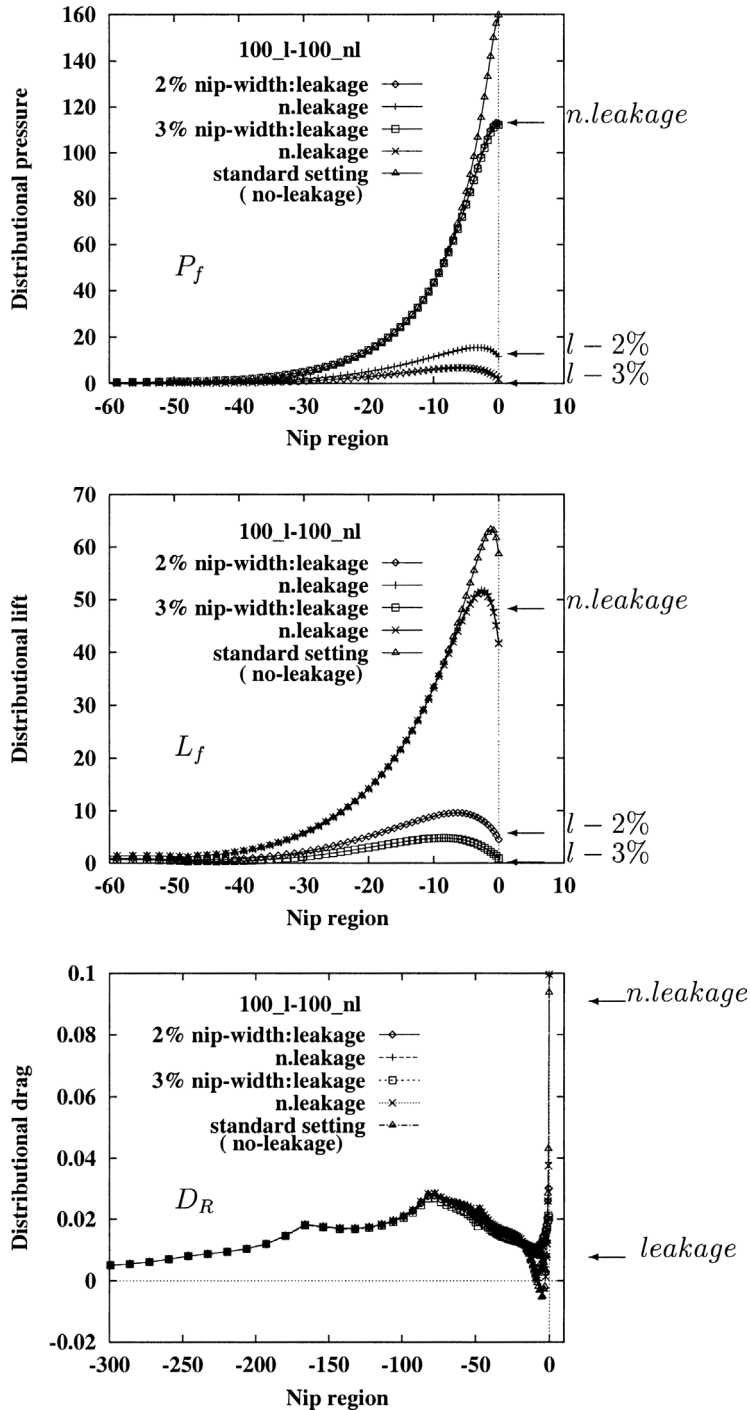


**Figure 11.** Global foil shifting, temporal variations, settled distributional pressure ( $P_f$ ) and lift ( $L_f$ ) on roller at  $L$  per cent nip-width of coat<sub>outlet</sub> 100<sub>l</sub>–100<sub>nl</sub> protocol

instabilities is demonstrated in Figure 15 on the coat-outlet layer and at the meniscus. These instabilities develop in time and reach a steady-state after long time periods. Such effects onset at the meniscus and propagate towards the coat-outlet region in time, see Figure 16. The amplitude of these oscillations enlarge with increasing nip-width. In Figure 15 oscillations are apparent on the free-surface. These would contribute to the final coating finish, rendering an uneven coating layer. The film-width would vary as a consequence, along the complete length of the sheet-foil. Over a leakage period, a slight decrease in the coat-outlet thickness arises to compensate and conserve flow rate. Free-surface profiles at meniscus and coat<sub>outlet</sub> regions for various nip-width settings are shown in Figure 16. In Figure 17, flow is presented in motion blur format at the various times of Figure 16 on the coat-outlet. At steady-state, a layer of uniform width is achieved, see Figure 17a. When the plate is allowed to move up and down in time by adjusting a nip-gap width, film-thickness varies along

**Table III.**  
Temporal leakage adjustment;  $P^{\text{mean}}$ , lift (on foil) and drag (on roller), values  $\times 10^3$  units

Protocol	$P^{\text{mean}}$	ampl.	Lift		Drag	
			leakage.	n.leakage.	leakage.	n.leakage
alternate $\Delta t$	157.9	0.05	1293	1296	1.279	1.305
$10_1 - 10_{\text{nl}}$	156.8	0.25	1293	1296	1.278	1.305
$20_1 - 50_{\text{nl}}$	157.3	0.55	1293	1299	1.278	1.305
$50_1 - 50_{\text{nl}}$	157.8	0.75	1300	1309	1.279	1.279
$100_1 - 100_{\text{nl}}$	157.8	1.25	1300	1309	1.279	1.280
std. Setting	159.8	–		1311		1.30

**Table IV.**  
Global foil shifting to steady state; maxima in  $P_{\text{nip}}$ , lift (on foil) and drag (on roller), values  $\times 10^3$  units

Nip-width % of coat-outlet	Leakage	$P_{\text{nip}}$	Lift	Drag
1%	Nil	160	1311	1.301
2%	0.0044	27	424	1.308
3%	0.0067	16	289	1.247

**Table V.**  
Foil shifting (globally); temporal force variations, values  $\times 10^3$  units

Force	Nip-width	$10_{\text{up}} - 10_{\text{reset}}$	$20_{\text{up}} - 50_{\text{reset}}$	$100_{\text{up}} - 100_{\text{reset}}$
Max $P_{\text{nip}}$	2%	31.5–57.6	37.8–102	11.5–113
	3%	15.6–46.8	17.4–94.6	1.9–113
	5%	2.2–38.6	8.5–88.8	–3.2–113
Lift (on foil)	2%	407.5–805	408.3–1128	277–1186
	3%	228.2–722	216.4–1096	136–1181
	5%	49.4–649	37.5–1071	13.1–1181
Drag (on roller)	2%	1.13–1.33	1.14–1.31	1.27–1.31
	3%	1.11–1.24	1.13–1.13	1.25–1.27
	5%	1.08–1.06	1.11–1.14	1.11–1.13

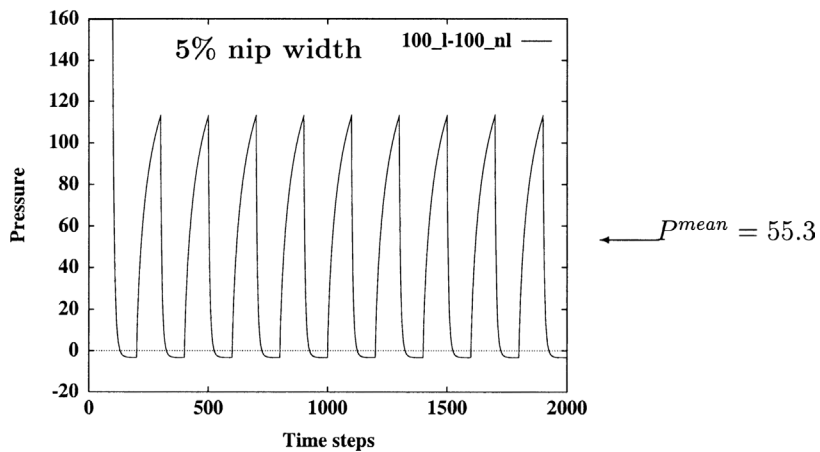
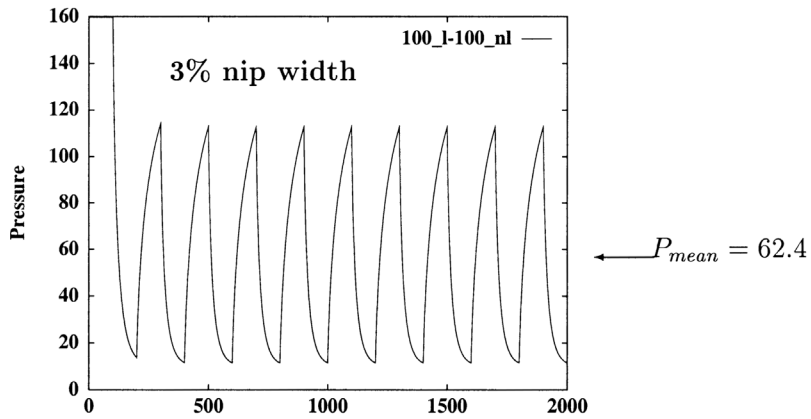
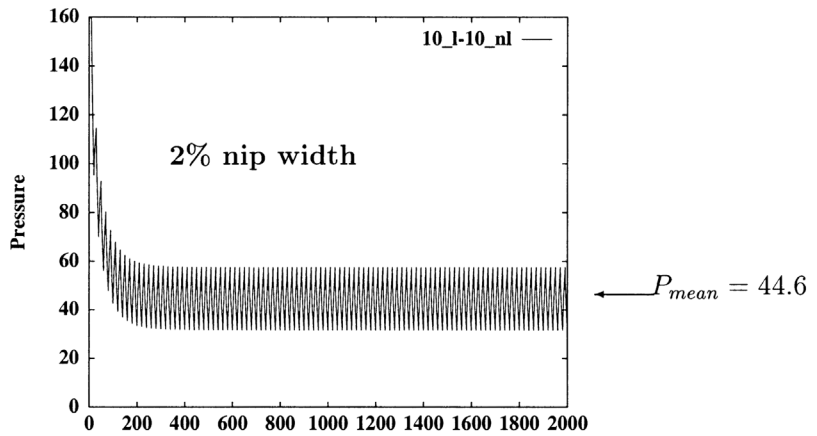


**Figure 12.**  
Global foil shifting;  
pressure ( $\times 10^3$ ) line  
plots at nip node  $N_1$ ,  $L$   
per cent nip width

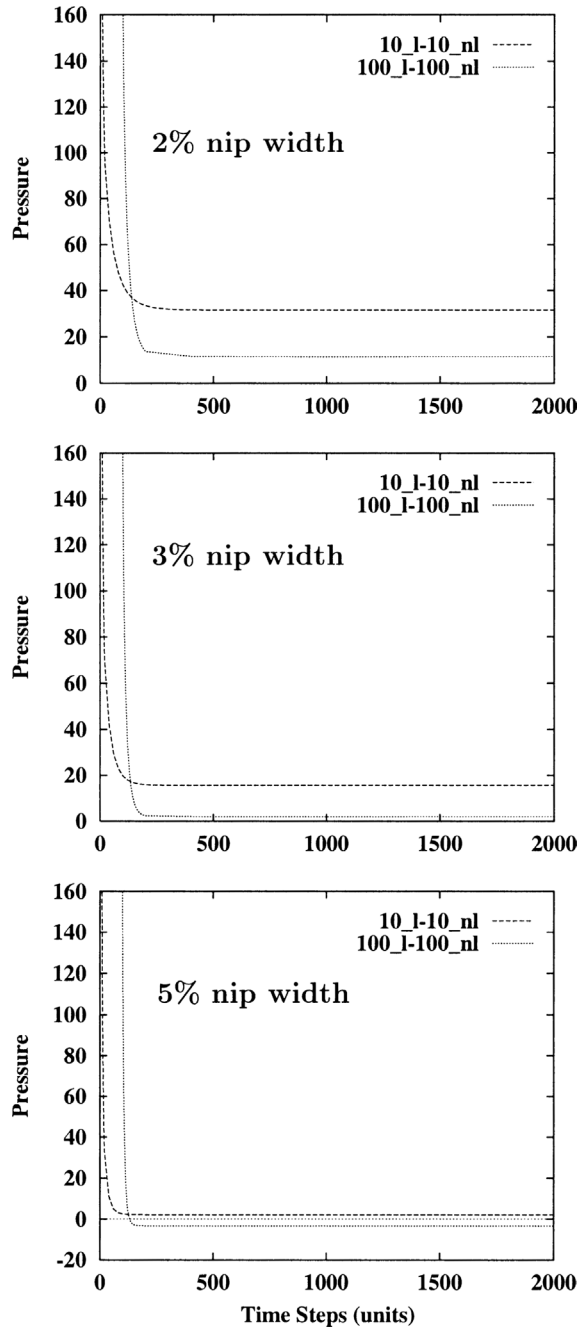


**Figure 13.**  
Global foil shifting;  
pressure ( $\times 10^3$ ) line  
plots at nip node  $N_1$ ,  
leakage state  $P_{\min}(t)$

---

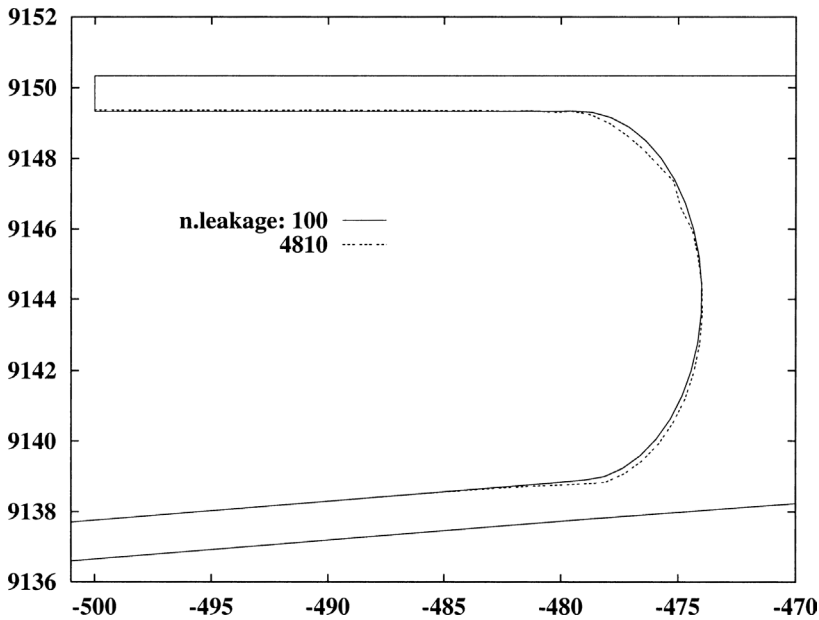


**Figure 14.**  
Global foil shifting; free-  
surface profile- full view

the strip length. An appropriate criterion is required to constrain the foil vibration, so that the pressure/lift generated remains within acceptable operating levels. We speculate that this may be achieved by selecting suitable leakage/no-leakage times.

#### 4.4 Temporal foil shifting (locally)

The motivation here is to discern whether foil vibration, local only to the nip, may have the same influence as that detected from global foil movement. Here, we are particularly concerned with lift and the adjustment of free-surface shape. The temporal solution response detected thus far, would indicate that local foil vibration may stimulate similar surface-finish fluctuations. Understanding the fundamental physical reasons behind such fluctuations is our goal.

In the preceding sections, it is observed that, the level of forces is fairly low along most of the foil/roller surfaces and rises significantly close to the nip region. Hence, the foil is shifted vertically upwards, in a local fashion, so that it takes up a linear slope of inclination within the nip region extending over a fraction of the foil length (30 per cent, 10 per cent, 4 per cent). Nip conditions are taken as of section 4.2. Maximum values of forces are charted below, and compared against those of section 4.3.1 with standard settings. We observe from Table VI and through Figures 17 and 18, that pressure and lift values,

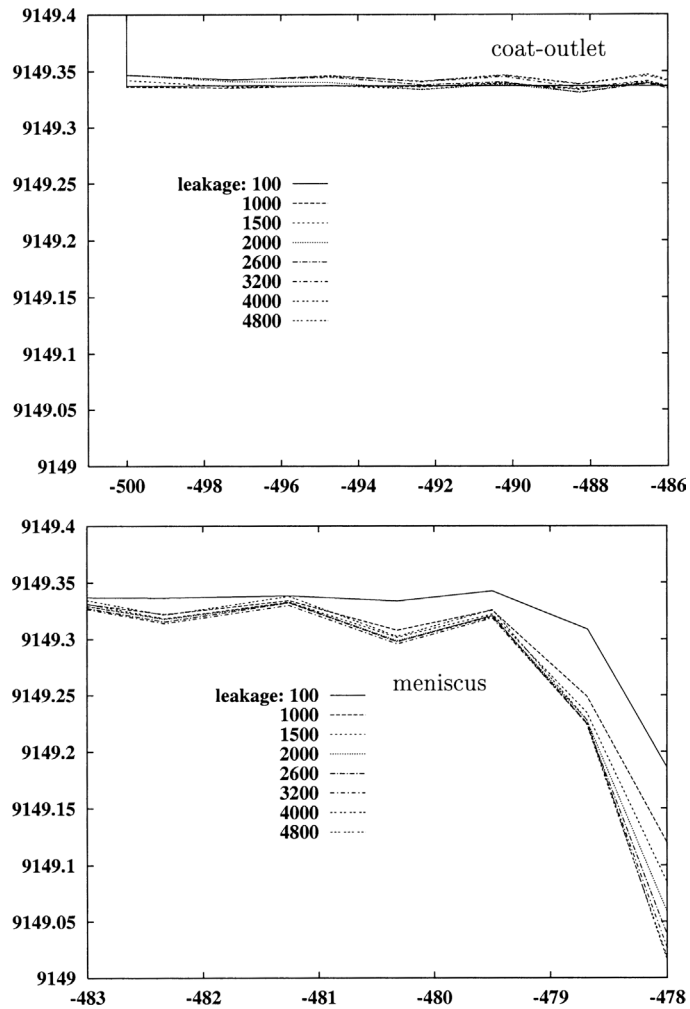


**Figure 15.**  
Global foil shifting;  
free-surface profiles-  
meniscus and coat-outlet;  
2 per cent nip-width,  
100<sub>l</sub>–100<sub>nl</sub> protocol,  
zoomed view at different  
time-steps

increase with decreasing length of the slope (approximating more closely to the standard setting). It is the elevation of peak values that varies between settings. The more local the foil shifting, the more elevated the peak pressures reached.

In the comparison of local versus global shifting, it is observed that the extent of disturbance from the nip coincides between global and local tests to within 10 per cent of the foil-length from the nip. This is true in all variables and for the standard no-leakage setting (i.e. time independent). Lift and drag also decrease. It is observed that, despite these differences in forces, both global

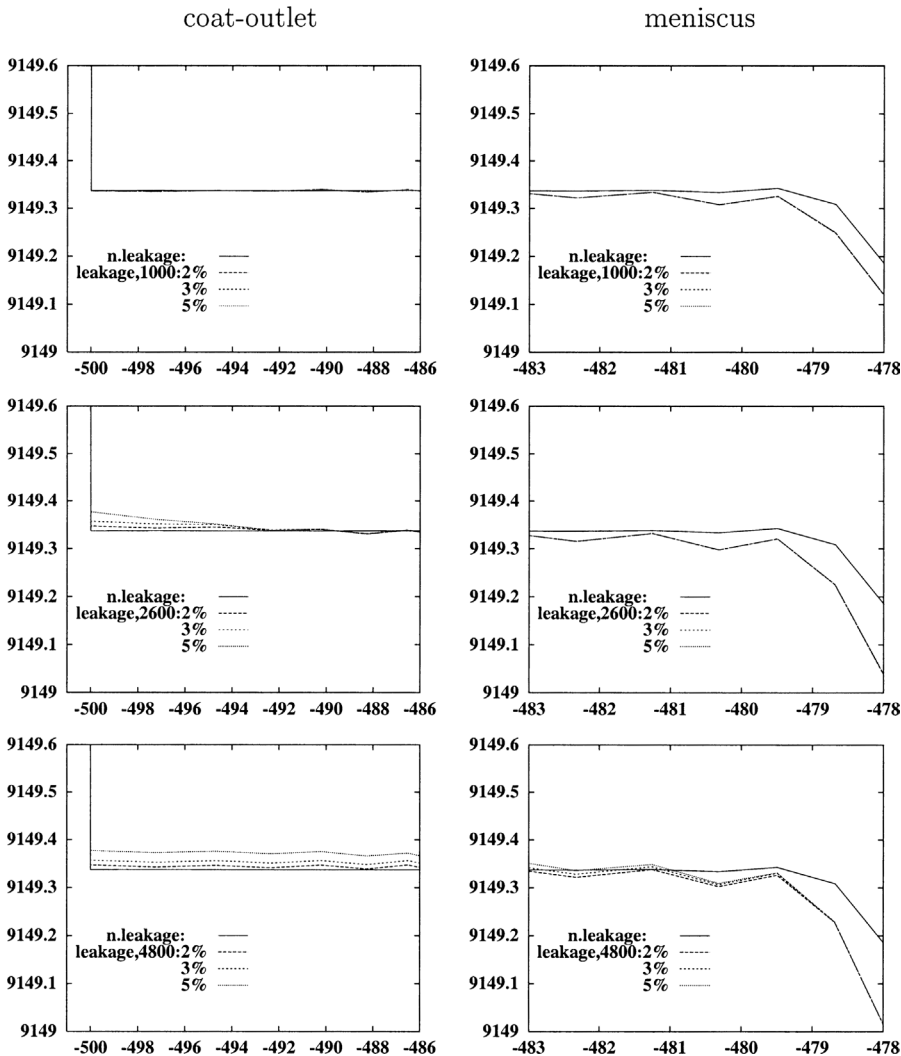


**Figure 16.** Global foil shifting; free-surface profiles, meniscus and coat-outlet; comparison at 2 per cent, 3 per cent and 5 per cent nip-width,  $100_1 - 100_{nl}$ , zoomed view; times 1000, 2600, 4800 (time step numbers)

and local settings have the same influence over the coat-outlet free-surface region, see Figure 19.

## 5. Conclusions

Generally, it is noted that when fluid travels on a coating roller, which is moving in the opposing direction to a foil, a pressure build-up will develop against whichever surface is moving with the greater differential speed. Under

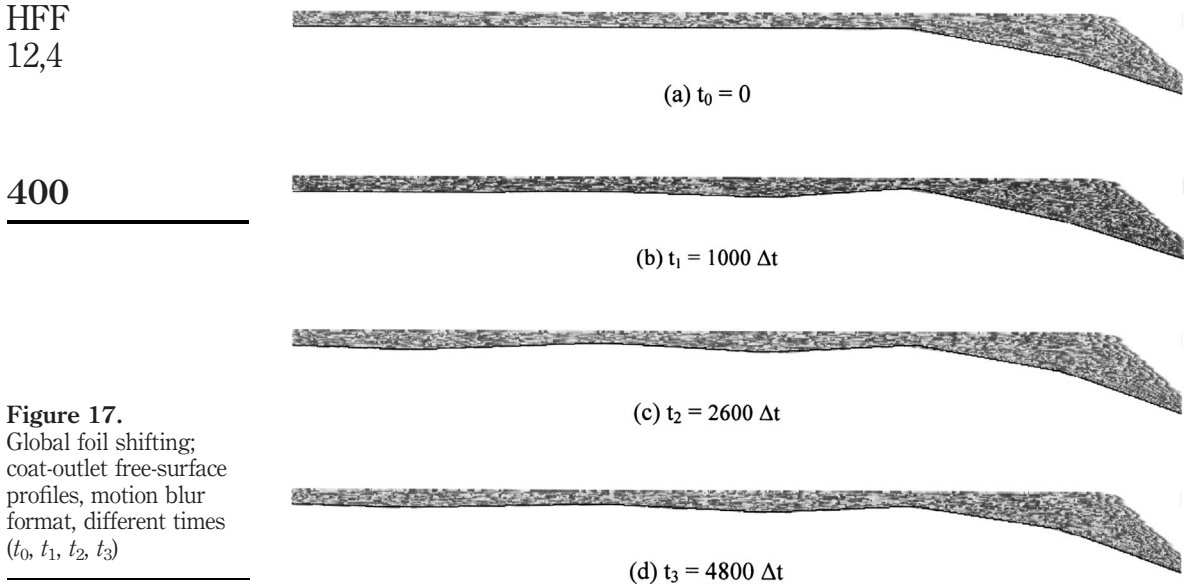


**Figure 17.**  
 Global foil shifting;  
 coat-outlet free-surface  
 profiles, motion blur  
 format, different times  
 $(t_0, t_1, t_2, t_3)$

**Table VI.**  
 Comparison  
 between global and  
 local foil-shifting, at  
 2 per cent nip-width,  
 $10_1 - 10_{nl}$  protocol

Force $\times 10^3$ units	Global foil-shifting	30% foil <sub>l</sub>	10% foil <sub>l</sub>	4% foil <sub>l</sub>	(Standard nl)
Max $P_{nip}$	31.5–57.6	71.5–83	81.0–88	105–110	160
Lift (on foil)	408.– 805	833–917.5	1025–1081	1191–1458	1311
Drag (on roller)	1.13–1.33	1.21–1.36	1.24–1.36	1.11–1.35	1.301

the present circumstances, it is generally the foil that moves with greater speed. When the pressure build-up reaches a threshold, the foil will rise away from the roller. This will create a widening of the gap (nip-width) between foil and roller. As a consequence, there will be relief of pressure that will act to bring the foil back down upon the roller. This sequence of events will generate temporal foil vibration. In this regard, a major observation of the present study emerges. Disturbances on the  $coat_{outlet}$  free-surface may be associated primarily with foil-vibration, either of a global or local nature. These oscillations begin at the meniscus free-surface region and propagate towards the  $coat_{outlet}$  region. Vibration in the free-surface profiles has been demonstrated at different time-step protocols, under various L per cent foil shifting, and in both leakage and no-leakage states. It is observed that the disturbance ratio factor on the  $coat_{outlet}$  free-surface is around 2 per cent for all leakage settings, once a settled periodic state has been established.

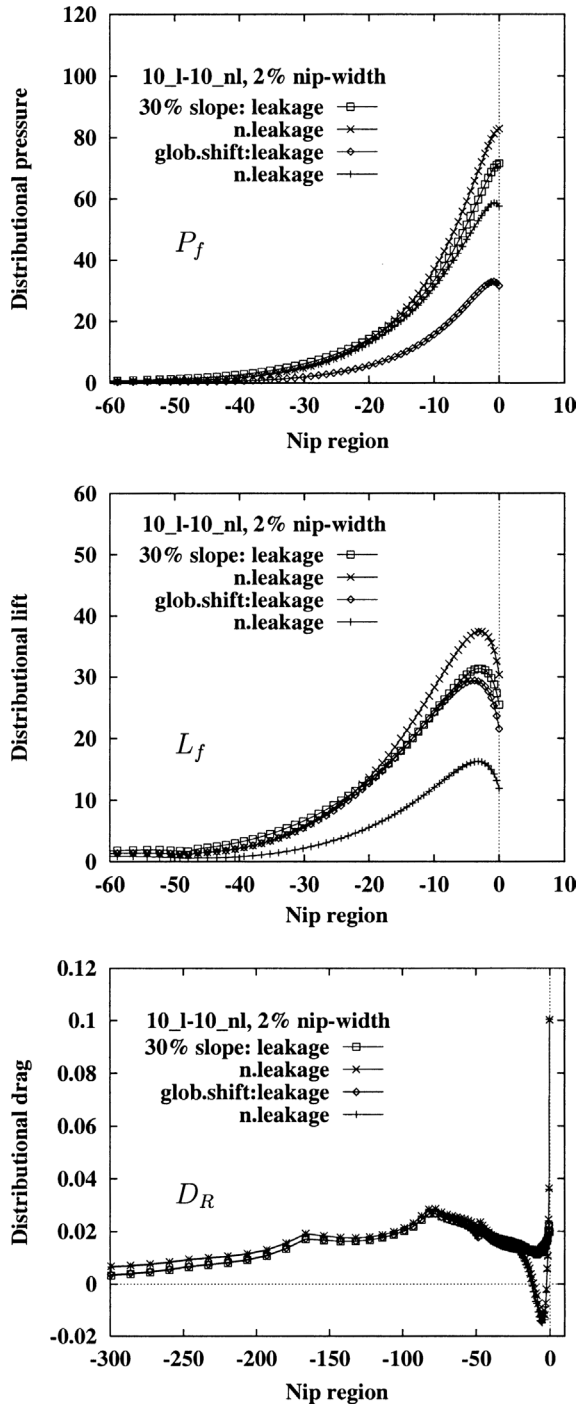


**Figure 18.**  
Comparison of settled  
distributional pressure  
( $P_f$ ) and lift ( $L_f$ ) along foil,  
and drag ( $D_R$ ) on roller;  
values  $\times 10^3$ : global foil  
shifting versus local foil  
shifting (slope over 30  
per cent of foil length)

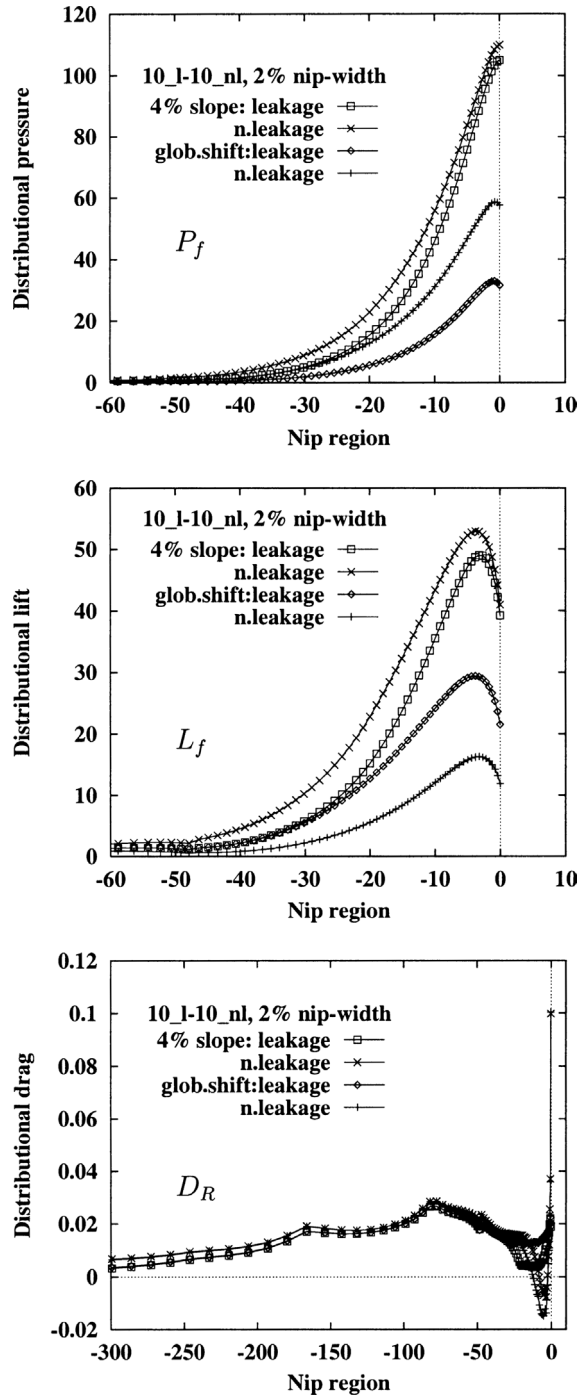


**Figure 19.** Comparison of settled distributional pressure ( $P_f$ ) and lift ( $L_f$ ) along foil, and drag ( $D_R$ ) on roller; values  $\times 10^3$ : global foil shifting verses local foil shifting (slope over 4 per cent of foil length)

**References**

- Benjamin, D.F. Roll Coating Flows and Multiple Flow Systems PhD. Thesis University of Minnesota, Minneapolis, MN, University Microfilms Int., Ann. Arbor, MI.
- Carvalho, M.S. and Scriven, L.E. (1997a), "Multiple States of a Viscous Free-Surface Flow: Transition from Pre-metered to a Metering Flow", *Int. J. Num. Meth. Fluids*, 24, pp. 813-31.
- Carvalho, M.S. and Scriven, L.E. (1997b), "Deformable Roll Coating Flows: Steady State and Linear Perturbation Analysis", *J. Fluid Mech.*, 339, pp. 143-72.
- Chandio, M. S. and Webster, M. F. *Numerical simulation of viscous free-surface flows for reverse roller-coating*, under review in *Int. J. Num. Meth. Heat Fluid Flow* (available as CSR 8-2001).
- Chen, K. S. A. and Scriven, L. E. *Roll Coating, Forward and Reverse: Effect of Feed Condition*; AIChE Spring Nat. Meet., New Orleans, LA 1988.
- Cohu, O. and Magnin, A. (1997), "Forward Roll Coating of Newtonian Fluids with Deformable Rolls: An Experimental Investigation", *Chem. Eng. Sci.*, 52 No. 8, pp. 1339-47.
- Carew, E.O.A., Townsend, P. and Webster, M.F. (1993), "A Taylor-Petrov-Galerkin Algorithm for Viscoelastic Flow", *J. non-Newtonian Fluid Mech.*, 50, pp. 253-87.
- Cuvelier, C., Segal, A. and Van Steenhoven, A. A., *Finite Element Methods and Navier-Stokes Equations*, D. Reidel, 1986.
- Fourcade, E., Bertrand, F., Régalt, O. and Tanguy, P.A. (1999), "Finite Element Analysis of Fluid-Solid Interaction in the Metering Nip of a Metering Size Press", *Comp. Meth. Appl. Mech. Eng.*, 174, pp. 235-45.
- Hawken, D.M., Tamaddon-Jahromi, H.R., Townsend, P. and Webster, M.F. (1990), "A Taylor-Galerkin Based Algorithm for Viscous Incompressible Flow", *Int. J. Num. Meth. Fluids*, 10, pp. 327-51.
- Hirt, C.W., Amsden, A.A. and Cook, J.L. (1974), "An Arbitrary Lagrangian-Eulerian Computing Method for All Flow Speeds", *J. Comp. Phys.*, 14, pp. 227-53.
- Keunings, R. (1986), "An Algorithm for the Simulation of Transient Visco-Elastic Flows with Free-Surfaces", *J. Comp. Phys.*, 62, pp. 199-220.
- Ramaswamy, B. (1990), "Numerical Simulation of Unsteady Viscous Free-Surface Flow", *J. Comp. Phys.*, 90, pp. 396-430.
- Regalt, O., Labrie, R. and Tanguy, P.A. (1993), "Free-surface Model for Dip Coating Process", *J. Comp. Phys.*, 109, pp. 238-46.
- Saito, H. and Scriven, L.E. (1981), "Study of Coating Flow by the Finite Element Method", *J. Comp. Phys.*, 42, pp. 53-76.
- Sato, T. and Richardson, S.M. (1994), "Numerical Simulation Method for Viscoelastic Flows with Free Surface-Fringe Element Generation Method", *Int. J. Num. Meths. Fluids*, 19, pp. 555-74.
- Silliman, W.J. and Scriven, L.E. (1980), "Separating flow near a static contact line: slip at a wall and shape of a free surface", *J. Comp. Phys.*, 34, pp. 287-313.
- Sizaire, R. and Legat, V. (1997), "Finite Element Simulation of a Filament Stretching Extensional Rheometer", *J. non-Newtonian Fluid Mech.*, 71, pp. 89-107.
- Townsend, P. and Webster, M. F. *An Algorithm for the Three-Dimensional Transient Simulation of non-Newtonian Fluid Flows*, Proc. NUMETA 87, Martinus Nijhoff, Dordrecht, vol. 2 T12/1 (1987).
- Tanner, R.I., Nickell, R.E. and Bilger, R.W. (1975), "Finite Element Method for the Solution of Some Incompressible non-Newtonian Fluid Mechanics Problems with Free Surfaces", *Comp. Meth. App. Mech. Eng.*, 6, pp. 155-74.